Proceedings of the 2001 DOE Hydrogen Program Review
NREL/CP-570-30535

GALLIUM NITRIDE INTEGRATED GAS/TEMPERATURE SENSORS FOR FUEL CELL SYSTEM MONITORING FOR HYDROGEN AND CARBON MONOXIDE

Stephen C. Pyke
Peterson Ridge, LLC
PO Box 1257
Sisters, OR 97759

Larry Sadwick
Department of Electrical Engineering
University of Utah
Salt Lake City, UT 84104

Abstract

Experimental results indicate the Pt-GaN-based FET (field effect transitor) gas sensors has the required sensitivity to measure the CO concentration in the 0-500 ppm range in H_2 and that the array concept for analyzing complex mixtures is more sensitive with increasing temperature >100˚C. The work leverages significant contributions in the literature on FET-based sensors on silicon and gallium nitride device electronics to extend the performance envelope for the FET-based gas sensor technology to high temperature. Results for the Pt and Rh catalytic gates at temperatures at and above 150˚C suggest a complex interaction of CO (51-1,014 ppm) and oxygen (0-5,000 ppm) and no saturation by hydrogen at 35vol%. The results are discussed in terms of the models currently used to describe the FET sensing mechanism.

Introduction

Gas sensing and analysis based on gas adsorption on a catalytic metal surface has been extensively explored using chemically sensitive semiconductor devices (Lundstrom 1989 and Spetz 1992). Recent work on field effect devices using catalytic metal gates on silicon carbide substrates has been reviewed (Spetz 1997 and Tobias 1997) and suggests the promising application of the field effect technology for high temperature gas monitoring. The limited use of large bandgap semiconductors for volume electronic applications has resulted in limited sources for devices for sensor applications. It is reasonable therefore to examine other high bandgap semiconductors as potential sources for high temperature sensors. Other materials in the III-V group of compound semiconductors are a potential source.

The field effect technology using catalytic metal electrodes on a semiconductor exploits chemisorption which is often dissociative (bond-breaking). The effect of hydrogen was reported first by Lundstrom (Lundstrom 1975) on a palladium gate field effect transistor (FET) on silicon. Later work demonstrated sensitivity to ethylene and carbon monoxide (Poteat 1983), hydrogen sulfide, propylene oxide, ethylene, formic acid, carbon monoxide and NO_2 (Hughes 1987). More recently, hydrogen, carbon monoxide, ethylene and acetylene effects have been observed on metal-insulator-semiconductor (MIS) capacitors with electrodes of pure platinum and platinum and palladium compositions with small amounts (ca. 5-10%) of transition metals such as copper, silver, and chromium (Feinstein 1997 and Pyke 1993).

There are two well-known hypotheses for how hydrogen and other gases are sensed by catalytically-active metal electrodes on FET sensors. Both hypotheses concur the change in work function alters the population distribution of carriers in the semiconductor under the metal by changing the surface potential of the semiconductor. In the first model, molecular hydrogen dissociates on the catalytic metal forming two adsorbed hydrogen atoms. Depending on their solubility and diffusivity, hydrogen atoms penetrate the metal to reach the metal-insulator or metal-semiconductor interface. In this model, only hydrogen alters the surface potential of the semiconductor covered with a solid electrode. The steady-state concentration of adsorbed hydrogen is mediated by reaction with other gases adsorbed on the surface, affecting the hydrogen concentration at the metal-insulator or metal-semiconductor interface. Thus, gases impacting the concentration of hydrogen on a catalytic surface can be measured only indirectly through the effect they have on hydrogen concentration at the metal-insulator or metal-semiconductor interface. In the second model, a perforated or porous solid electrode adsorbs gas as in the first model, however it is proposed the dipole field-produced hydrogen changes the surface potential of the semiconductor without diffusion into the metal (Dobos 1990, Hedborg 1994 and Lundstrom 1996). The dipole field is proposed to result from adsorbates at the edges of the perforations or pores. A similar but more aggressive design to expose more of the metal surface facing the semiconductor used a suspended metal electrode (Cassidy 1986). By etching away a sacrificial metal layer deposited between the dielectric and the catalytic metal, a cavity is produced which is accessible to gas. Perforations in the suspended metal allow any gas to penetrate to the cavity and adsorb on the metal facing the semiconductor. In principle, nearly the total underside surface is available for any gas to adsorb and produce the dipole field and so influence the surface potential of the semiconductor.

GaN High Temperature Electronics

Owing to their wide bandgap, the III-V nitrides are attractive for high-temperature, high-power electronics applications. Forming low contact resistivity, thermally stable and uniform ohmic contacts constitutes a major obstacle for wide band gap materials such as GaN. With a band gap about 3.4 eV, Ga-N is therefore, receiving increased attention. GaN-based devices and circuits have the potential to operate at 600°C or higher temperatures. For GaN and other highly ionic semiconductors, evidence has suggested that the Schottky barrier height of metal to III-nitride contacts strongly depend on the difference between the work function of the metal and the electron affinity of the semiconductors. It is fairly easy for metals with lower work functions to form ohmic contacts on n-GaN. This explains why Ti, Al, W, and Cr are chosen as ohmic contacts on n-GaN. Similarly, metals with higher work functions, such as Pt, Rh and PdAg, are expected to form good Schottky barriers (necessary for high impedance contact and low leakage current) to n-GaN.

As with other semiconductor systems, especially compound semiconductor systems, the formation of an alloyed semiconductor/contact is usually the most straightforward method to achieve "ohmic" behavior. This is most certainly true for other group III-V semiconductors such as the well-studied and characterized GaAs semiconductor. Almost all known, successful contacts to III-V semiconductors consist of bi-level to multi-level metallization schemes. The interface between the semiconductor and the first metallization layer is the most important, for it controls the transport mechanism(s). Usually, chemical or thermal reactions, solid-state diffusion and interdiffusion, and/or other methods produce mixing, due possibly to material damage (i.e., ion mixing and ion implantation). The key is to find some species, usually an element, that reacts with the respective substitutional dopant and either the group III or group V element to form an alloy of variable composition such that transitions occur from semiconducting to semimetallic to metallic. This type of contact, essentially, forms a tunneling ohmic contact with linear I-V characteristics. An example of this is the Au-Ge-Ni ohmic contact to n-type GaAs.

Among the several metals studied for ohmic contacts on n-GaN, Pd/Al and Ti/Al were found to have the lowest specific contact resistances. The formation of Pd/Al on n-GaN has been reported (Ping 1996), whose specific contact resistance was found to be 1.2×10^{-5} ohm-cm^2 upon annealing at 650°C for 30 seconds. A significant improvement with Ti/Al on n-GaN was obtained (Lin 1994), who employed a Ti/Al bilayer deposited by e-beam evaporation followed by rapid thermal annealing (RTA) at 900°C for 30 sec in N_2 ambient. A specific contact resistance of 8×10^{-6} ohm-cm^2 was reported. One recently proposed ohmic metallization scheme involved Ti/Al-based composites, namely Ti/Al/Ni/Au (150•/2200•/400•/500•) preceded by a reactive ion etching (RIE) process that most likely rendered the surface highly n-type (Fan 1996). After annealing at 900°C for 30s, specific contact resistance of 1×10^{-7} ohm cm^2 for a doping level of 4×10^{17}cm^{-3} was obtained. Unfortunately, Au reacted with GaN during the annealing.

Lin et al. found specific contact resistance of Ti/Al metallization suffered from Ga outdiffusion and subsequent reaction with Al rendering the surface metal discontinuous and increasing its resistance. A second sequence of Ti/Al was added (Wu 1995) following the annealing step, to

minimize the high resistivity problem. Ohmic-specific contact resistance was lowered to ~$3x10^{-6}$ ohm cm^2.

Pt, Rh and PdAg as Catalytic Gate Materials

Platinum and palladium were selected because each has shown sensitivity in the ppm range for ethylene, acetylene and carbon monoxide. Both metals are also PROX catalyst candidates, and both metals have been used as Schottky junctions on GaN. PdAg was selected, because the mechanical integrity is better than pure Pd at these hydrogen concentrations. Rhodium was selected, because of its PROX catalytic activity and to help resolve the effects of the multiple gases in combination with platinum and PdAg. Each of these metals is expected to adsorb CO preferentially in the fuel stream just as in the PROX catalyst. It was surmised the reaction of CO and hydrogen with oxygen on the surface of the catalyst produces a steady-state surface composition that can be detected through the work function change of the catalyst. The higher affinity for CO in preferential catalysis also suggests the three metals should show sensitivity for carbon monoxide even in the presence of a great excess of hydrogen.

Experimental

Fabrication

We have successfully fabricated Schottky contacts using platinum, palladium/silver and rhodium. We used process technology that has resulted in contacts that only a few of which have survived without delamination. The gate metals were applied to a variant of the MESFET called a MODFET for modulation-doping-field-effect-transistor. The architecture is shown in Figure 1. The gates are the two strips at the centers of the two FETs on the left. Each gate is bounded by a source and drain ohmic contact.

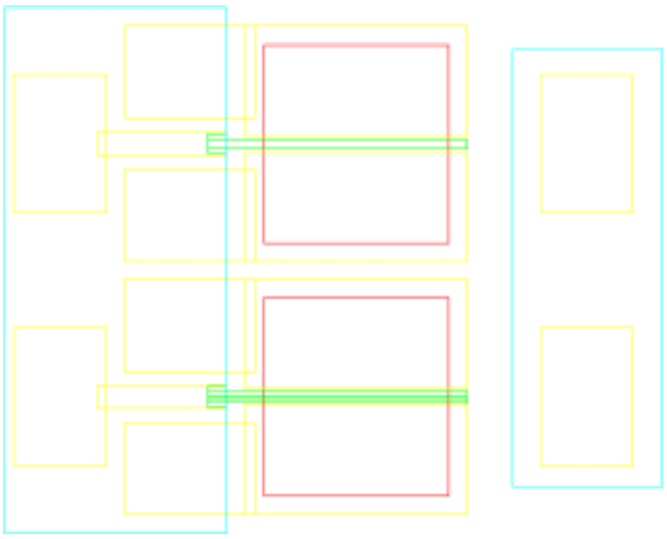

Figure 1: FET Sensor Architecture showing two FETs. The right-hand feature is a set of bonding pads for thermocouples.

Two gate designs (single and dual strips) were fabricated. The collocation of the single and dual gate on the wafer makes for the closest match in electrical properties for the most accurate comparison of the gas effect.

The design dimensions and the actual dimensions are shown in Table 1 below.

Table 1: Dimensions of FET Sensors

	Single Gate		Dual Gate		No Gate
	Design	Actual	Design	Actual	Design
Gate Length	200 • m	200 • m	200 • m	200 • m	200 • m
Ohmic Contacts	20000 • m^2		20000 • m^2		20000 • m^2
Gate Metal Width	10 • m	8.6 • m	2x5 • m	2x4.25 • m	n/a
Gate Metal Area	2000 • m^2	1920 • m^2	2000 • m^2	1900 • m^2	n/a
Drain-Gate	3~4 • m	5 • m	2 • m	3.5 • m, 3.7 • m	n/a
Drain-Source	17 • m	18.7 • m	17 • m	18.7 • m	17 • m
Intergate spacing	n/a		3 • m	3.1 • m	n/a
Gate Area Exposed	1400 • m^2	2030 • m^2	1400 • m^2	2050 • m^2	3400 • m^2
Ratio of Gate Exposed to Covered	0.7	1.06	0.7	1.08	n/a
Ratio of Gate Edge to Area	0.2 • m^{-1}	0.21 • m^{-1}	0.4 • m^{-1}	0.42 • m^{-1}	

The actual dimensions were determined from the transmission electron microscope (TEM) micrograph shown in Figure 2 below and the scanning electron microscope (SEM) micrograph of the single gate in Figure 3.

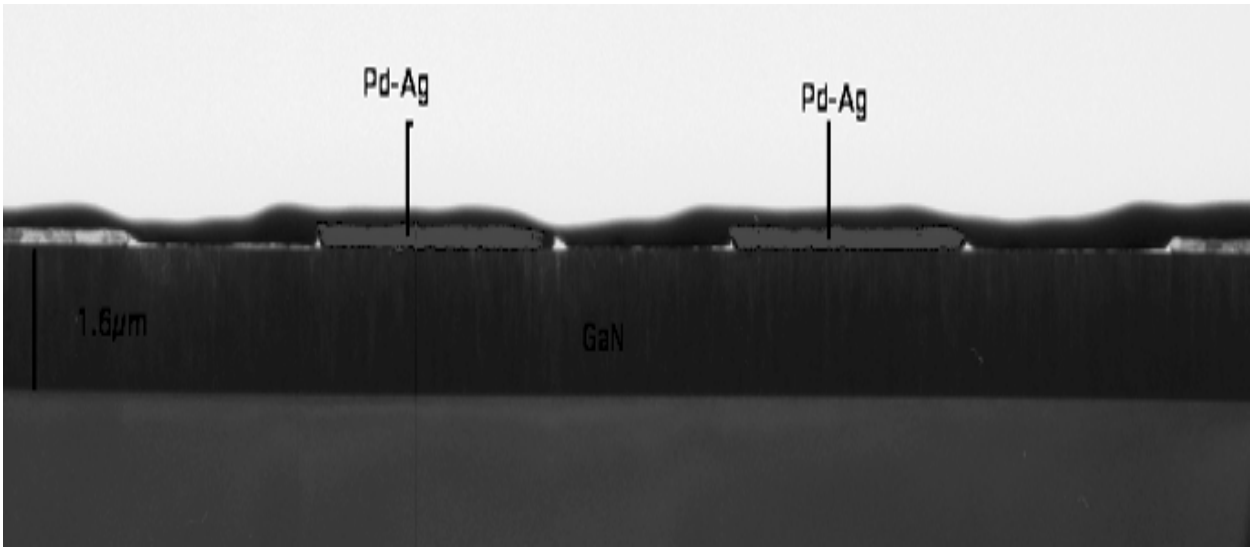

Figure 2: TEM photomicrograph of the crossection of the dual gate device.

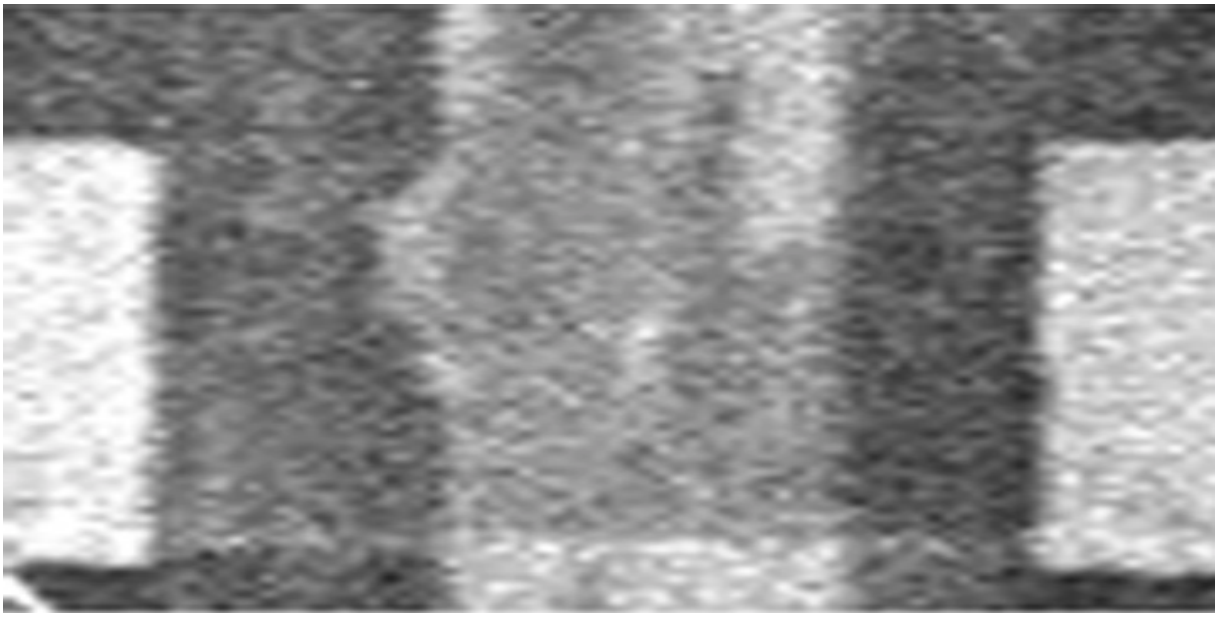

Figure 3: SEM micrograph of a representative single metal gate.

The metal thickness for PdAg was measured in the TEM image shown in Figure 4. The film thickness proposed (ca. 50-100 nm) was expected to be an island type film (e.g. where the films become discontinuous). There is no evidence of porosity or pinholes. The film is continuous and appears densely packed.

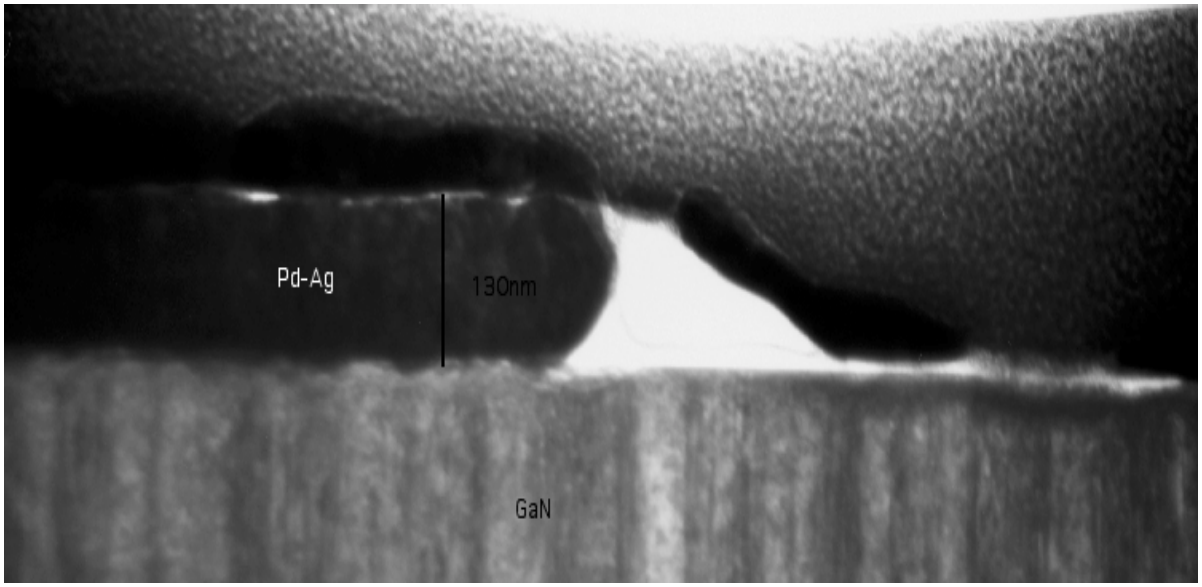

Figure 4: TEM micrograph of the PdAg with film thickness of 130 nm.

All of the metallization was carried out at the University of Utah. All metals were deposited by e-beam evaporation at the Hedco Laboratory at the University of Utah. Following the deposition, all sensors were subjected to annealing at 600°C for 5 minutes in the vacuum chamber. All three gate metals exhibited poor adhesion (Figure 5.) Only four working PdAg sensors were fabricated – all of these on one test article.

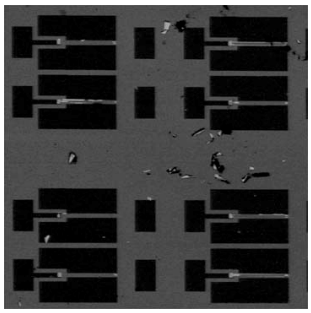

Figure 5: Rhodium sensor showing catastrophic delamination of the gate metal typical of the first fabrication run of these devices.

The sensors supplied by U. Utah include five with no gate (for reference), four with PdAg, eight with Rh and six with Pt. The pad assignments and electrical characteristics are shown in Figure 6.

Sample : No - Gate
Gate :

Device #	Drain or Source Pad #	Gate Pad #	Id max @V_{ds} = 20 V	Single or Dual Gate
1	7,8		23.88 mA	Un-gated
2	9,10		24.37 mA	Un-gated
3	11,12		25.56 mA	Un-gated
4	16,17		23.30 mA	Un-gated
5	18,19		21.42 mA	Un-gated
6				

Sample : Rh Up
Gate : Rhodium

Device #	Drain or Source Pad #	Gate Pad #	Id max @V_g = +1.5 V @V_{ds} = 15 V	Single or Dual Gate
1	5,7	4	34 µA	D
2	8,9	24	492 µA	S
3	10,11	14	366 µA	S
4	15,21	20	31.4 µA	D
5				
6				

Sample : Pd - Ag Up
Gate : PdAg

Device #	Drain or Source Pad #	Gate Pad #	Id max @V_g = +1.5 V @V_{ds} = 15 V	Single or Dual Gate
1	12,16	13	1.29 mA	D
2	17,18	10	2.1 mA	S
3	21,22	8	1.93 mA	S
4	23,24	7	1.29 mA	D
5				
6				

Sample : Rh DWN
Gate : Rhodium

Device #	Drain or Source Pad #	Gate Pad #	Id max @V_g = +1.5 V @V_{ds} = 15 V	Single or Dual Gate
1	6,7	5	40.5 µA	S
2	3,16	2	28.8 µA	D
3	8,9	10	189.5 µA	S
4	11,12	14	40.6 µA	D
5				
6				

Sample : Pt - Right
Gate : Platinum

Device #	Drain or Source Pad #	Gate Pad #	Id max @V_g = +1.5 V @V_{ds} = 15 V	Single or Dual Gate
1	11,12	14	1.50 mA	D
2	7,9	10	3.92 mA	D
3	18,20	19	2.40 mA	D
4	21,23	22	4.72 mA	S
5				
6				

Sample : Pt - Left
Gate : Platinum

Device #	Drain or Source Pad #	Gate Pad #	Id max @V_g = +1.5 V @V_{ds} = 15 V	Single or Dual Gate
1	11,18	17	5.24 mA	S
2	9,10	8	4.52 mA	D
3				
4				
5				
6				

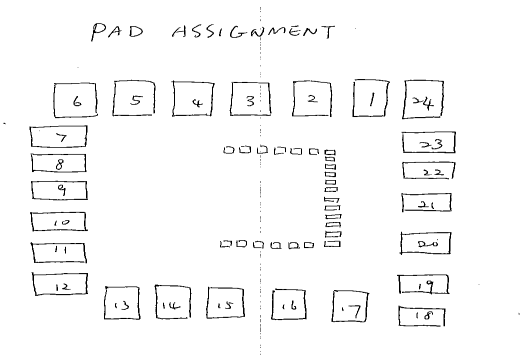

Figure 6: Listing of the pad assignments and device electrical characteristics of each of the devices

Sensor Electronics

Sensor electronics were designed to operate FET sensors at a constant source drain current. As changes in the gate voltage due to gas exposure change the source drain current, a feedback voltage equal and opposite to the gas effect is applied to the gate. The field gradient between the gate metal and the GaN can cause migration of charged species that result in long-term changes in the baseline electrical properties of the device. The potential for long term changes (drift) is reduced if the field remains constant. The circuit elements are shown in Figure 7.

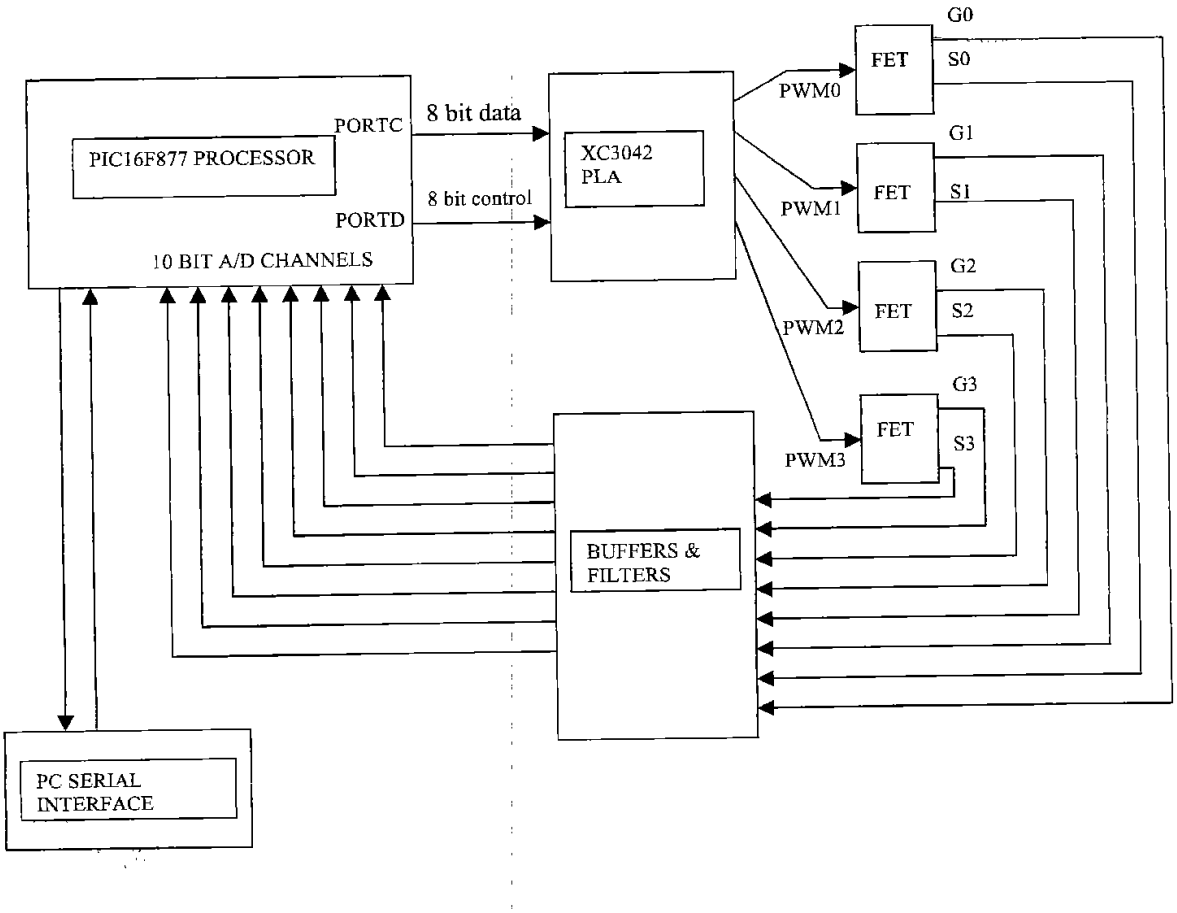

Figure 7: Block diagram of the constant current constant voltage sensor drive circuit.

The system consists of a MicroChip PIC 16F877 RISC controller, XYLINX XC3042 PLA, and unity gain buffers for the A/D interface used to maintain constant source current with up to four MODFETs or MESFETs. The PIC contains eight 10-bit A/D channels. Four channels are used to monitor FET source current (1 per FET). The other 4 channels are used to monitor FET gate voltage. The XC3042 is programmed to contain four 12-bit pulse width modulators (PWMs) that are used to control gate voltage. The PWMs are buffered using Analog Devices AD823 OP-AMPS. The PWMs are filtered using 2 pole R/C pi filters that have a pole frequency of 1 Hz.

The circuit is programmed through an RS232 connection with a terminal program (Hyperterminal on the data PC). The drain source voltage is a constant 12V. The unit searches

for the gate voltage to achieve the target source drain current. When the unit finds this gate voltage, it locks each sensor so that only external changes to the gate voltage or source drain current cause the output voltage to the gate metal to change.

Sensor Test Design

Testing in gas was done with the sensor in a quartz chamber (shown in Figure 8) heated by infrared radiation from quartz halogen lamps.

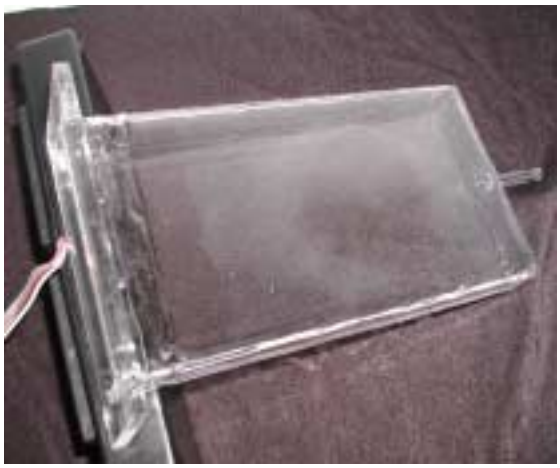

Figure 8: Sensor chamber showing exhaust tube at the right.

An aluminum plate with a Buna rubber gasket was clamped to the flange. Sensor wires, gas and thermocouple connections were made through penetrations in the aluminum plate and sealed with high-temperature RTV.

Data were obtained by poling four sensor gate voltages and four source voltages using a CIO-DAS16/Jr data acquisition board for the PC from Computerboards, Middleboro, MA. Data were logged by a program called vlogger and stored as a time-tagged text file. The text files were imported into Microsoft Excel and charted. We used two standard charts for data analysis. The first was an x-y plot of gate voltage versus time. The second chart was a 3-D surface chart with the x-axis showing CO concentration, the y-axis showing O_2 concentration and the z-axis showing the measured gate voltage.

Results

Surface and Interface Chemical and Structural Analysis

Focused ion beam trenching and TEM and X-ray analysis scanning across freshly exposed interfaces were performed. The data suggest little interdiffusion as close to the interface as 125 • . An unexpected result was that the Pd/Ag atomic ratios suggest substantial surface segregation of Ag. Both the lower surface near the GaN and the upper surface show

approximately 50-60% decrease in the Pd/Ag atomic ratio in the bulk from about 2:1 Pd:Ag to about 1:1 Pd:Ag at the surface. This is surprising in that both surfaces show similar effects suggesting little if any chemical or mechanical effect of the different interfaces. The surface energy and resulting reorganization in the annealing process is more consistent with the observation of a weak bond with the GaN and little or no Pd or Ag in the GaN quite near the interface.

The TEM and X-ray results show little or no interdiffusion of Rh with GaN. The rhodium material is thinner than the PdAg and shows evidence of less than theoretical density (see Figure 9).

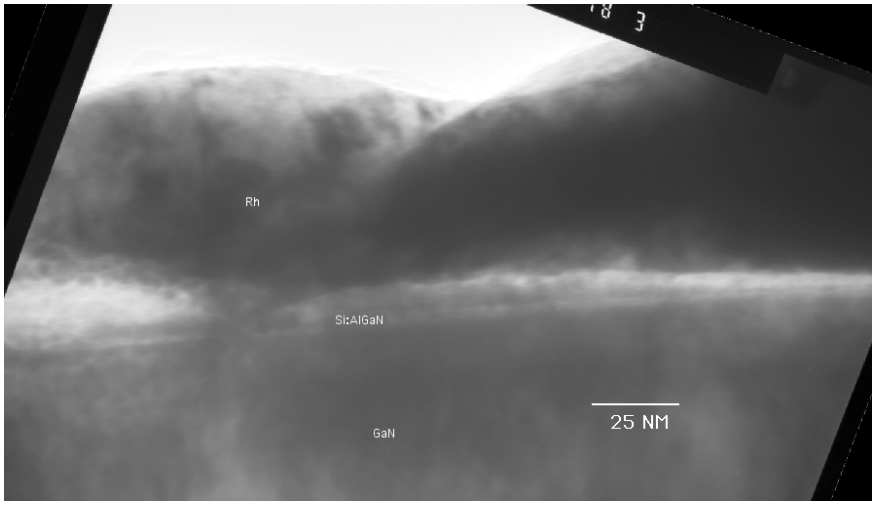

Figure 9: TEM of Rhodium film.

The Rh showed no interdiffusion with GaN within the resolution limit of the analysis (ca. 125•). The annealing treatment during fabrication was at a temperature much higher than that seen by any of the sensors during gas testing.

Gas Testing

Sensors were fabricated on sapphire substrates and dye attached to glass for easier electrical connection and are shown in Figure 10.

Gas exposure experiments were run at temperatures T•125•C. The gas concentration was varied by adjusting the duty cycles of a system of valves connected to a mixing manifold and controlled by a PC (See Table 2). The O_2, CO and balance gases were all 35.0•0.1%(vol) hydrogen. The O_2 standard was 2.0•0.1%(vol) O_2 and the CO standard was 2010•10 ppm. All gases were analyzed and certified by Scott Specialty Gas.

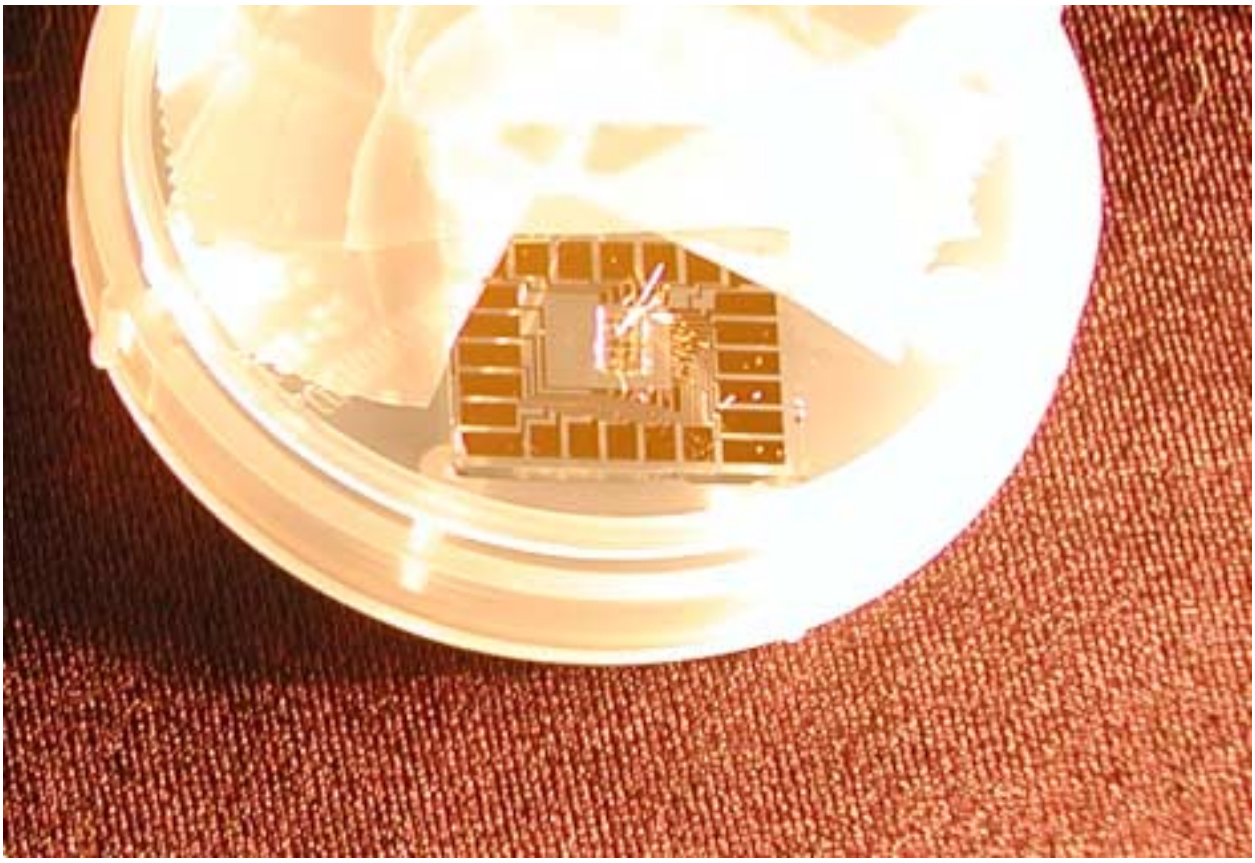

Figure 10: Sensor packaging.

Table 2: Order of experiments.

Total Flow (SCCM)	O_2 (SCCM)	CO (SCCM)	Balance (SCCM)	$[O_2]$ppm	[CO]ppm	p
600	300	15	285	5000	51	
600	300	300	0	5000	1015	
600	300	150	150	5000	507	
600	50	150	400	833	507	
600	50	300	250	833	1015	
600	50	15	535	833	51	
600	0	300	300	0	1015	
600	0	150	450	0	507	
600	0	15	585	0	51	

The flow rates of gases in Table 2 are in standard cubic centimeters per second.

Gate Voltage Versus Time

Initial experiments were performed on the PdAg sensor with each of the standard gas blends. Temperature was controlled by switching two 500-W quartz halogen lamps located above and

below the sensor chamber. Switching was accomplished by a CN4800 temperature controller and SSRDUAL240DC40 solid-state relay, Omega, Stamford, CT. A thermocouple (J-type) was bonded to the bottom of the glass sensor package. The thermocouple voltage was input to the CN4800 controller to maintain a constant temperature. Temperature fluctuations at the set point were less than •1•C. Voltage changes were in the range of 20 mV for PdAg for all exposures shown in Table 2 up to 125•C. There was typically greater sensitivity to the target gases with an increase in temperature for the Rh and Pt sensors. Unfortunately, the PdAg wire bonds were damaged prior to testing above 125•C. The highest temperature attained with the experimental test equipment was 200•C for the Rh results shown in Figure 11.

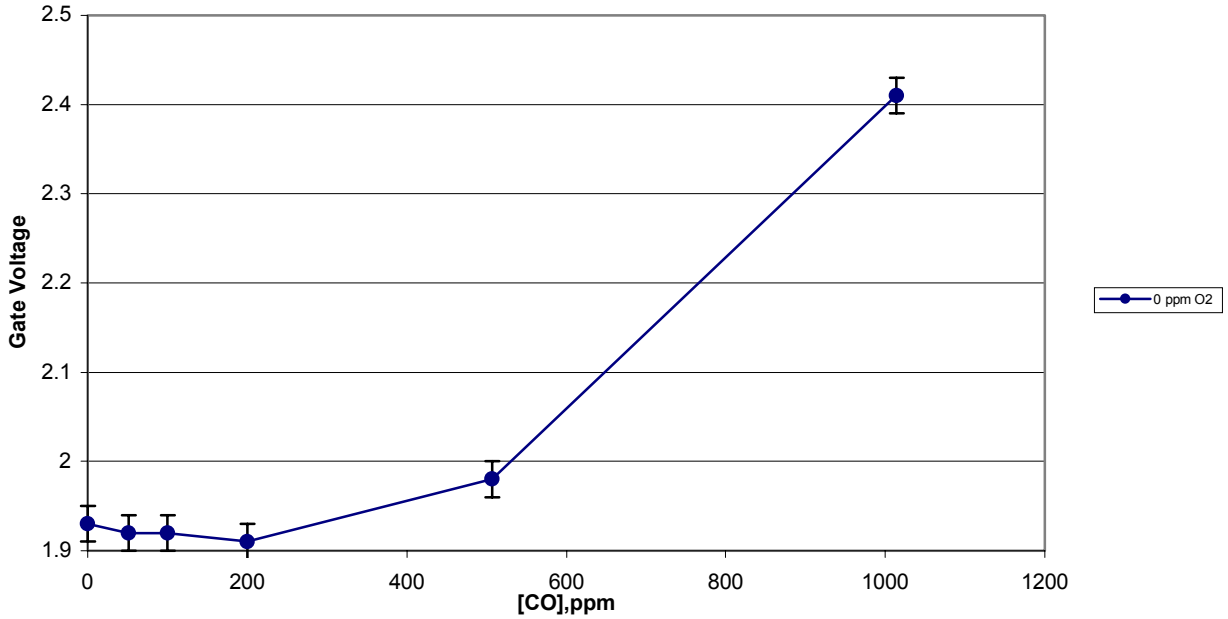

Figure 11: Rh sensor response to CO at zero ppm O_2 and 200•C

The data for Rh show substantially more sensitivity at 50•C on the dual gate sensors. By 150•C, all of the Rh sensors were showing the same response pattern with a maximum of 0.2V change in gate voltage compared with 0.3V change for Pt at 1014 ppm CO. At 200•C, the Rh sensor response increases significantly.

Experimental Results in CO and O_2

We constructed surface plots for results on Pt sensors showing the main effects of the two concentration variables on the gate voltage at 50•C, 100•C and 150•C (Figures 12, 13 and 14, respectively). We can also qualitatively assess the interaction effects of one concentration variable on the other. These results are shown below.

Both the single and dual gate responded in a similar pattern, with the dual gate more sensitive at low levels of CO (ca. <500 ppm) at 150•C. Neither has CO sensitivity in the target region of

low levels (ca. <500 ppm) until 150•C. At 100•C, the sensitivity to CO at 5,000 ppm O_2 changes sign compared to 0 ppm O_2.

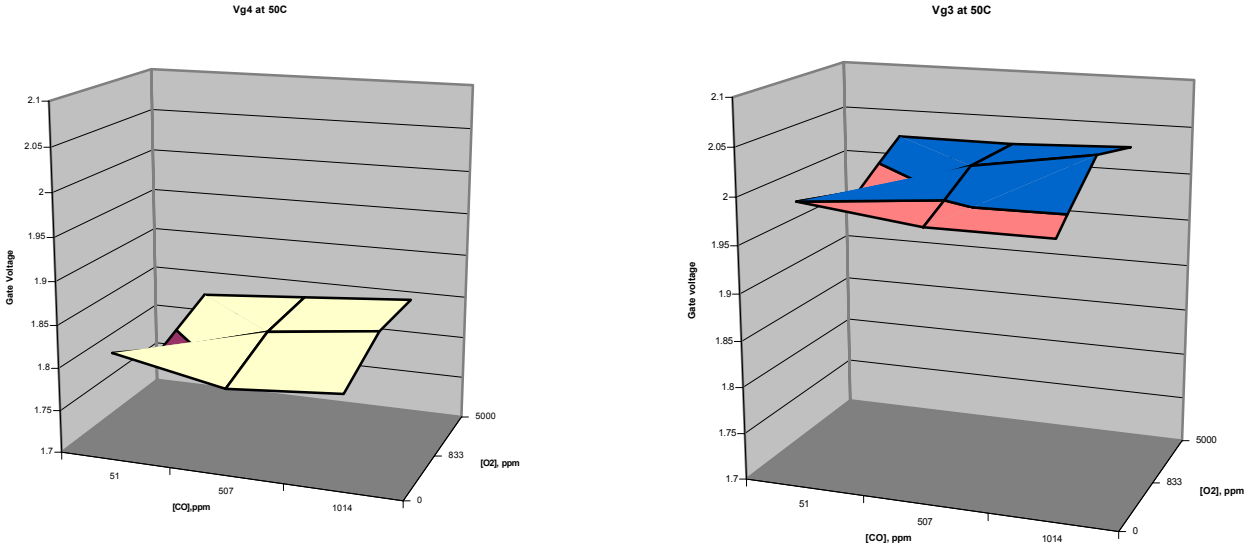

Figure 12: Single gate response on left. Dual gate response right. Both at 50•C.

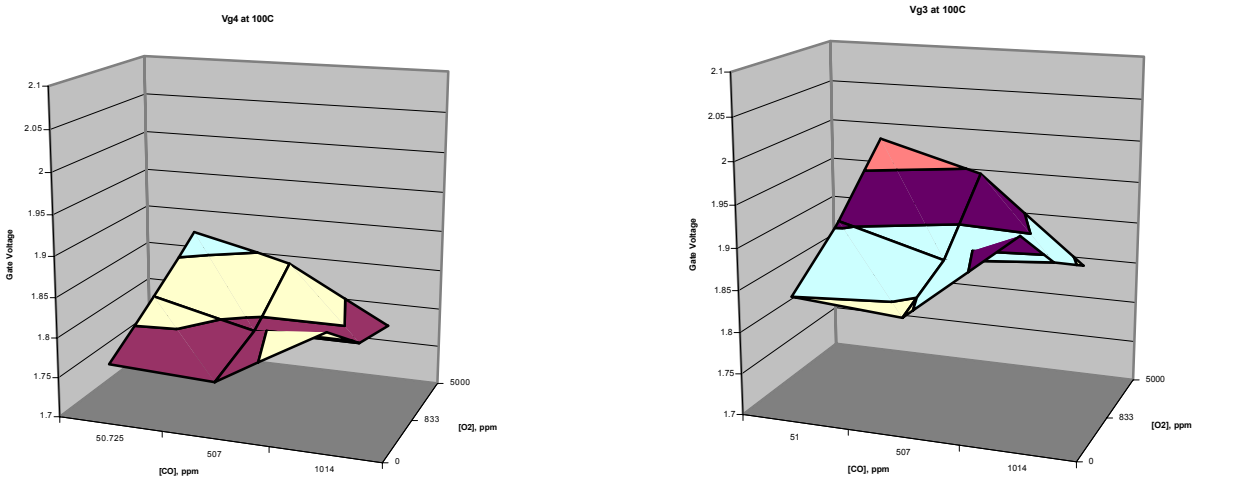

Figure 13: Single gate response on left. Dual gate response right. Both at 100°C.

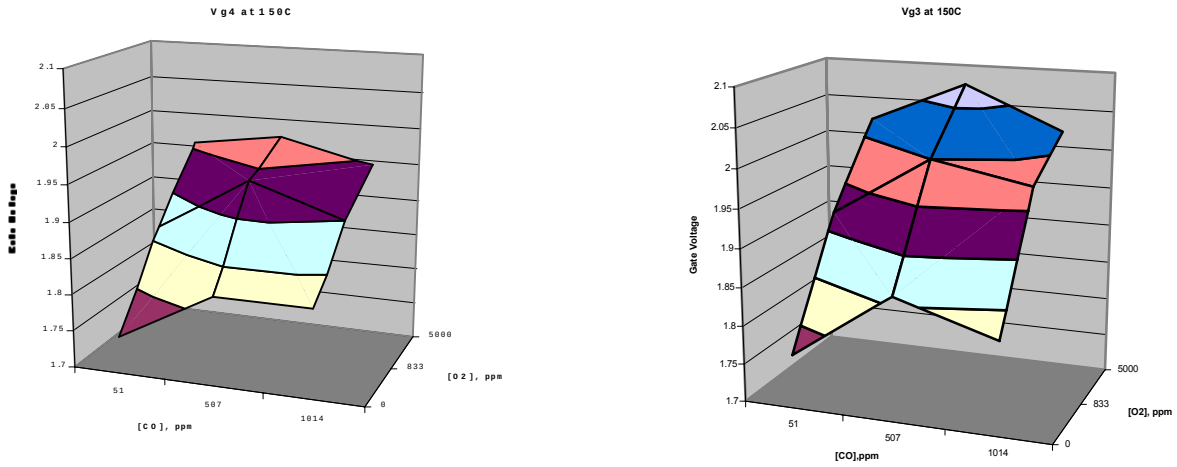

Figure 14: Single gate response on left. Dual gate response on right. Both at 150°C

Discussion and Conclusions

The strongest conclusions we can draw are: 1.) the gate Pt and Rh do not mix with the GaN up to 600 • C (5 minutes in vacuum), and mixing would not be a likely source of long-term drift in performance; 2.) little intermixing means poor adhesion and a poor manufacturing yield; 3.) high hydrogen concentration (35vol%) does not poison the sensor to ppm levels of CO; 4.) the O_2 sensitivity is comparable to the sensitivity to CO; 5.) the dual gate design shows greater sensitivity to CO and O_2 at temperatures >100 • C; and 6.) the potential exists for sensing CO below 500 ppm in pure H_2 using catalytic gate FET sensors (i.e. with a separate sensor selective for CO or O_2, the CO and O_2 concentrations can be resolved assuming a simple mixture of H_2 and CO with only O_2 as an interferent). Since other contaminants are likely in H_2 fuel from carbon based-fuel sources, additional testing with other potential interferents is necessary and at higher temperatures in order to determine the performance of a sensor array based on the GaN FET sensor.

A tentative conclusion can be drawn that the improved sensitivity is the result of the dual gate over the single gate design. There is a twofold greater edge length of the dual gate over the single gate designs and is consistent with the model that more than hydrogen can adsorb and cause a direct change in the device performance. How the adsorption alters the field inside the semiconductor is an issue that begs further study.

Acknowledgments

The authors would like to acknowledge the support provided by the DOE Hydrogen Program through contract no. G010453. The authors are also grateful for the design and fabrication assistance of Howard Chern at the University of Utah, Randy Sindelar for electronics design and Jack McCarthy at OGI for microscopy.

References

Cassidy, J., S. Pons and J. Janata. 1986 Anal. Chem., 58:1757.

Dobos, A.K., et al. 1990. Sensors and Actuators, B1:25

Fan, Z., S.N. Mohammad, W. Kim, O. Aktas, A.E. Botchkarev, K. Suzue, and H. Morkoc. 1996. J. Electronic. Materials, 25:1703.

Feinstein, D.I., C. Renn, M. Scharff and S.C. Pyke. 1997 "Metal-Insulator-Semiconductor (MIS) Gas Sensor Array for Gas Analysis and Diagnosing Faults in Oil-Filled Power Transformers," 191st Meeting of the Electrochemical Society, Montreal, Quebec, Canada.

Hedborg, E., F. Winquist, and I. Lundstrom. 1994. Appl. Phys. Lett., 64(4):420.

Hughes, R.C., W.K. Schubert, T.E. Zipperian, J.L. Rodriguez and T.A. Plut. 1987. J. Appl. Phys., 62:1074.

Lin, M.E., Z. Ma, F.Y. Huang, Z.F. Fang, L.H. Allen, and H. Morkoc. 1994. Appl. Phys. Lett., 64:1003.

Lundstrom, I., M.S. Shivaraman, C. Svensson, and L. Lundqvist. 1975. J. Appl. Phys., 26:55.

Lundstrom, I., M. Armgarth and L.-G. Petersson. 1989. CRC Critical Reviews in Solid State and Materials Sciences, 15:201-278.

Lundstrom, I., and L.G. Petersson. 1996. J. Vac. Sci. Technol., A, 14(3):1539.

Niessen, A.K., and A.R. Miedema. 1983. Ber. Bunsenges. Phys. Chem., 87:717 and references therein.

Ping, A.T., M. Asif Khan and I. Adesida. 1996. J. Electronic. Materials, 25:819.

Poteat, T.L., B. Lalevic, B. Kuliyev, M. Yousef and M. Chem. 1983. J. Electron. Mater., 12:181.

Pyke, S.C. 1993. "Transformer Fault Gas Analyzer," (invited paper) First Annual EPRI Substation Equipment Diagnostic Conference, Palo Alto, CA.

Spetz, A.L., F. Winquist, H. Sundgren and I. Lundstrom. 1992. "Field Effect Gas Sensors," in G. Sberveglieri (ed.), Gas Sensors, Kluwer, Dordrecht, 219-279.

Spetz, A.L., A. Baranzahi, P. Tobias and I. Lundstrom. 1997. Phys Stat. Sol. (a) 162:493-511.

Tobias, A. Baransahi, A. Lloyd-Spetz, O. Kordina, E. Janzen and I. Lundstrom. 1997. IEEE Electron Device Letters, 18:287-289.

Wu, Y., W. Jiang, B. Keller, S. Keller, D. Kapolnek, S. DenBarrs and U. Mishra. 1995. Topical Workshop on III-V Nitrides, Nagoya, Japan.